

# A Spiral Scaffold Underlies Cytoadherent Knobs in *Plasmodium falciparum*-Infected Erythrocytes

Short title: Adherent knobs in malaria-infected erythrocytes

Jean M. Watermeyer<sup>1</sup>, Victoria L. Hale<sup>1</sup>, Fiona Hackett<sup>2</sup>, Daniel K. Clare<sup>1</sup>, Erin E. Cutts<sup>3</sup>, Ioannis Vakonakis<sup>3</sup>, Roland A. Fleck<sup>4</sup>, Michael J. Blackman<sup>2</sup> and Helen R. Saibil<sup>1\*</sup>

<sup>1</sup>Department of Biological Sciences, Birkbeck, University of London, London, United Kingdom;

<sup>2</sup>The Francis Crick Institute, Mill Hill Laboratory, London, United Kingdom; <sup>3</sup>Department of Biochemistry, University of Oxford, Oxford, United Kingdom; <sup>4</sup>Centre for Ultrastructural Imaging, Kings College, London, United Kingdom

\* Corresponding author: Helen R. Saibil

Department of Biological Sciences

Birkbeck, University of London

Malet Street, London

WC1E 7HX

Email: h.saibil@mail.cryst.bbk.ac.uk

Tel. +442076316820

Fax. +442076316803

Text words: 3988; Abstract words: 242; Figures: 7; Tables: 0; References: 75

24 **Key Points:**

25

- 26 • *P. falciparum*-generated cytoadherent knobs on infected erythrocytes contain a
- 27 spiral framework linked to the red cell cytoskeleton
- 28 • The findings suggest a structural basis for transmission of shear forces in
- 29 adhesion of infected cells

## Abstract

Much of the virulence of *Plasmodium falciparum* malaria is caused by cytoadherence of infected erythrocytes, which promotes parasite survival by preventing clearance in the spleen. Adherence is mediated by membrane protrusions known as knobs, whose formation depends on the parasite-derived, knob-associated histidine-rich protein (KAHRP). Knobs are required for cytoadherence under flow conditions, and they contain both KAHRP and the parasite-derived erythrocyte membrane protein PfEMP1. Using electron tomography, we have examined the three-dimensional structure of knobs in detergent-insoluble skeletons of *P. falciparum* 3D7 schizonts. We describe a highly organised knob skeleton composed of a spiral structure coated by an electron dense layer underlying the knob membrane. This knob skeleton is connected by multiple links to the erythrocyte cytoskeleton. We used immunoelectron microscopy to locate KAHRP in these structures. The arrangement of membrane proteins in the knobs, visualised by high resolution freeze fracture scanning electron microscopy, is distinct from that in the surrounding erythrocyte membrane, with a structure at the apex that likely represents the adhesion site. Thus, erythrocyte knobs in *P. falciparum* infection contain a highly organised skeleton structure underlying a specialised region of membrane. We propose that the spiral and dense coat organise the cytoadherence structures in the knob, and anchor them into the erythrocyte cytoskeleton. The high density of knobs and their extensive mechanical linkage suggest an explanation for the rigidification of the cytoskeleton in infected cells, and for the transmission to the cytoskeleton of shear forces experienced by adhering cells.

54 **Introduction**

55

56 *Plasmodium falciparum* malaria remains one of the leading causes of child deaths globally,  
57 with the majority of cases occurring in sub-Saharan Africa and South-East Asia. While  
58 chemopreventive and vector control initiatives led to an estimated 42% reduction in  
59 mortality rates between 2000-2012, the emergence of artemisinin resistance highlights the  
60 importance of continued efforts to understand and interfere with the biology of the parasite <sup>1</sup>.

61

62 Of the five *Plasmodium* species capable of infecting humans, *P. falciparum* and *P. vivax* are the  
63 most prevalent, with *P. falciparum* causing 90% of malaria-related deaths. *P. falciparum*-  
64 infected erythrocytes become cytoadherent, causing erythrocyte sequestration in the  
65 microvasculature and avoiding clearance of infected cells by the spleen <sup>2</sup>. Much of the  
66 virulence of *P. falciparum* malaria has been attributed to this cytoadherence, which impedes  
67 blood circulation, and results in severe syndromes such as cerebral or placental malaria <sup>2-4</sup>.

68

69 The dominant ligand mediating cytoadherence is PfEMP1, a major variable erythrocyte  
70 surface antigen of *P. falciparum* which may interact with a number of different host receptors  
71 <sup>2,3,5</sup>. Clonal antigenic variation of PfEMP1, encoded by the *var* multi-gene family, has been  
72 proposed to be responsible for adherence to different tissues, and hence for variations in  
73 disease progression <sup>6,7</sup>. PfEMP1 isoforms are recognised by antibodies that provide variant-  
74 specific immunity to *P. falciparum* <sup>3</sup>. One variant, VAR2CSA, which binds to chondroitin  
75 sulphate in the placenta causing pregnancy-associated malaria, has been identified as a  
76 vaccine target <sup>8</sup>. PfEMP1 is presented on the outside of infected erythrocytes, where it is  
77 localised to the surface of membrane protrusions known as knobs <sup>4,9-11</sup>. These knobs appear  
78 as prominent bumps on the surface of infected erythrocytes, from the early trophozoite stage

79 onwards <sup>10,12,13</sup>. PfEMP1 is transported to knobs via Maurer's clefts <sup>14</sup>. Disruption of genes  
80 required for PfEMP1 trafficking to the membrane **causes** dramatic reductions in  
81 cytoadherence <sup>15,16</sup>. Loss of the ability to form erythrocyte knobs has been linked with a loss  
82 of parasite virulence in primate infections <sup>17</sup>, **and** with reduced cytoadherence *in vitro* <sup>15,18,19</sup>.  
83  
84 The formation of the PfEMP1-presenting knobs is dependent on the expression of the  
85 parasite-derived knob-associated histidine-rich protein (KAHRP). Erythrocytes infected with  
86 KAHRP-negative *P. falciparum* lack knobs and show diminished PfEMP1 presentation and  
87 reduced adherence to CD36, ICAM-1 and CSA under flow conditions <sup>18-20</sup>. KAHRP is localised  
88 with PfEMP1 in knobs <sup>18,21</sup> where it has been shown by immuno-EM to be associated with an  
89 electron-dense (as visualised in heavy-metal stained specimens) layer of material under the  
90 membrane, as well as in Maurer's clefts <sup>22,23</sup>. KAHRP is a 59-72 kDa protein (550-657 amino  
91 acid residues depending on the variant) containing an N-terminal signal sequence and a  
92 PEXEL (*Plasmodium* export element) motif that mediate export into the erythrocyte, a 63-  
93 amino-acid histidine-rich (55%) region, and two variable tandem repeat **regions** <sup>24-26</sup>.  
94 Expression of KAHRP has been shown **to increase the** rigidity of infected erythrocytes,  
95 thereby further contributing to cytoadherence-associated virulence <sup>27</sup>. This rigidifying effect  
96 on the cytoskeleton **is** common to a number of exported parasite proteins <sup>15,27</sup>. Use of gene  
97 knock-out mutants has revealed that in addition to KAHRP, two genes, those encoding a  
98 PHIST domain protein (PFD1170c), and an Hsp40-like DNAJ Type IV protein (PF10\_0381), are  
99 also important for knob formation <sup>15</sup>. Other parasite proteins that have been shown to  
100 associate with knob components, and which may thus form part of the knob structure, include  
101 knob-associated Hsp40 <sup>28</sup>, the PfEMP1 trafficking protein PfEMP3 <sup>16,28</sup>, the large variable  
102 surface antigen SURFIN <sup>29</sup>, the 2.5 MDa Pf332 antigen <sup>30</sup> and the PHIST domain protein  
103 PFE1605w (LyMP) <sup>31,32</sup>. PFE1605w is localised at the cell periphery <sup>33</sup> and has been shown to

104 be important for cytoadherence but not for knob formation or for surface expression of  
105 PfEMP1 <sup>31</sup>.

106

107 We have examined the architecture of cytoadherent knobs in *P. falciparum* 3D7-infected  
108 erythrocytes. By isolating the erythrocyte cytoskeletons of mature schizonts, we have found a  
109 distinctive spiral structure with an electron-dense coat underlying the knob membrane. This  
110 knob skeleton is anchored into the surrounding erythrocyte cytoskeleton, which connects to  
111 the electron-dense coat. Freeze-fracture scanning electron microscopy (SEM) shows that the  
112 arrangement of membrane proteins in the knobs is quite distinct from that in the surrounding  
113 erythrocyte membrane, with a structure at the apex that may represent the site of adhesion.  
114 We propose that the knob skeleton provides a mechanical linkage between the adhesion site  
115 and the cytoskeleton.

116

117

## 118 **Methods**

119

### 120 *P. falciparum* culture

121 *P. falciparum* 3D7 asexual blood stages were maintained in human erythrocytes in RPMI 1640  
122 medium containing Albumax (Thermo Fisher Scientific, Waltham, MA, U.S.A.), with  
123 synchronisation using standard methods <sup>34</sup>. Human blood was obtained with full consent  
124 from the UK National Blood Transfusion service, and was used within 2 weeks of receipt.  
125 Enrichment of mature schizonts was achieved using Percoll (GE Healthcare, Little Chalfont,  
126 UK) as described previously <sup>35</sup>.

127

### 128 High pressure freezing and freeze substitution

129 Mature schizonts were pelleted by centrifugation, mixed with RPMI medium containing  
130 brewer's yeast and dextran as a cryoprotectant, and high-pressure frozen in aluminium  
131 planchettes using an HPM010 high pressure freezer (BalTec, Reading, UK). This material was  
132 freeze-substituted into HM20 resin (Polysciences, Inc., Warrington, PA, U.S.A.) containing  
133 0.2% uranyl acetate. 200-220 nm sections were cut using an EMUC7 ultramicrotome (Leica  
134 Camera AG, Wetzlar, Germany) fitted with a diamond knife, and mounted on carbon-coated  
135 copper grids. Grids were then coated with 10 nm protein-A gold (Sigma-Aldrich, St. Louis, MO,  
136 U.S.A.) as a fiducial marker for tomography.

137

#### 138 Preparation of schizont skeletons for negative-stain and cryo-tomography

139 Cytoskeletons of schizonts and uninfected erythrocytes were prepared *in situ* on carbon-  
140 coated copper grids as follows. Grids were glow-discharged, coated with 0.01% poly-L-lysine  
141 (Sigma-Aldrich) for 30 seconds, washed with water and blotted dry. Grids for cryo-  
142 tomography were additionally coated with 10 nm colloidal gold fiducial markers (Sigma-  
143 Aldrich). Mature schizonts or uninfected erythrocytes in phosphate-buffered saline (PBS;  
144 approx. 20% haematocrit) were applied to the grids, allowed to adhere for 1 minute, then  
145 blotted from the back and washed once with PBS. Grids carrying cells were dipped  
146 sequentially into lysis buffer (1 mM Tris pH 4.7, 1 mM KCl, 0.2 mM MgCl<sub>2</sub>), lysis buffer  
147 containing 2% Triton X-100, and then lysis buffer without detergent to wash, for 60 seconds  
148 in each solution, passing through the meniscus several times. Grids were then either stained  
149 with 2% sodium silicotungstate, pH 7.5, blotted and air-dried, or blotted from the back and  
150 plunge-frozen in liquid ethane using a manually operated apparatus.

151

#### 152 Immunolabelling

153 Schizont and uninfected erythrocyte skeletons were prepared on grids as described above,  
154 then immunolabelled while still wet before staining or plunge-freezing. KAHRP was detected

155 using monoclonal antibody (mAb) 89<sup>22</sup> or mAb 18.2 (anti-KAHRP, obtained from the  
156 European Malaria Reagent Repository, donated by Dr. Jana McBride), followed by goat anti-  
157 mouse secondary antibody doubly conjugated with 10 nm gold and Alexafluor 488 (Thermo  
158 Fisher Scientific). Spectrin was detected using antibody ab11751 (Abcam, Cambridge, UK),  
159 and gold-conjugated secondary antibody as above. Antibodies were diluted in blocking buffer  
160 (0.5% cold water fish skin gelatine (Sigma-Aldrich), 1% normal goat serum (Thermo Fisher  
161 Scientific), 0.05% Tween-20 in PBS). Grids were incubated for 30 minutes each in blocking  
162 buffer, followed by primary antibody solution, then secondary antibody solution. Grids were  
163 washed in PBS between steps, and in low salt buffer before negative staining as described  
164 above. For controls, primary antibody was omitted from the second incubation step, or  
165 replaced with preimmune serum.

166

#### 167 Transmission electron microscopy

168 Images and tomograms of resin-embedded and negative stained skeletons were collected  
169 using an FEI T12 electron microscope with a tungsten filament operated at 120 kV, or an FEI  
170 F20 electron microscope operated at 200 kV. A US4000 CCD camera (Gatan, Abingdon, UK)  
171 was used for imaging. Dual-axis tomograms were collected using a dual-tilt tomography  
172 holder (E.A. Fischione Instruments, Inc., Export, PA, U.S.A.).

173 Cryo-tomograms were collected from vitrified specimens 100-300 nm thick using a Polara  
174 electron microscope operated at 300 kV (FEI Company, Hillsboro, OR, U.S.A.), equipped with a  
175 Quantum energy filter and a K2 direct electron detector (Gatan). Zero loss filtering was  
176 carried out using a 20 eV slit width. Images were collected in electron counting mode with  
177 dose fractionation, using 3-6-second exposures with 6-20 subframes per exposure. Total  
178 exposures were 60-110 electrons per square Angstrom ( $e^-/\text{\AA}^2$ ) for cryo-tomograms and 200-  
179 270  $e^-/\text{\AA}^2$  for negative-stain dual-axis tomograms. Tomographic tilt-series collection was  
180 controlled using Serial EM<sup>36</sup>.



181

182 Image processing

183 Tomographic reconstruction and subframe alignment were carried out using IMOD <sup>37</sup>. 5 or 10  
184 nm gold beads were used as fiducial markers, and some tomograms were aligned by patch  
185 tracking. Gold particles in tomographic reconstructions were detected automatically using  
186 IMOD findbeads3d, knobs were modelled using 3dmod, and the relative spatial distribution of  
187 gold and knobs was calculated using IMOD MTK <sup>37</sup>. The average densities of gold beads  
188 calculated by MTK for individual tomograms were combined by weighting the tomogram  
189 average according to the number of knobs present. Gold beads in images of immunolabelled  
190 material were counted automatically using ImageJ. Tomograms were denoised for display  
191 using nonlinear anisotropic diffusion (NAD) filtering.

192

193 Freeze-fracture scanning electron microscopy

194 Mature schizonts were concentrated by centrifugation, high-pressure frozen as above without  
195 additional cryo-protectant, then fractured at -110 °C and multi-axis rotary coated at high  
196 vacuum with a 4 nm layer of chromium using a BAF060 freeze fracture system fitted with a  
197 VCT100 vacuum cryo transfer system (BalTec). Samples were imaged under cryo-conditions  
198 using a specialised semi in-lens cryo-SEM (JSM-7401F, JEOL (UK) Ltd, Welwyn Garden City,  
199 UK) equipped with a cold-source field emission gun, beam deceleration and an energy filter.  
200 Images were collected using low beam landing energy (1.2 kV) at 37000 - 60000x  
201 magnification and a working distance of 4-5.4 nm.

202

203 Database depositions

204 Representative tomograms have been deposited in the Electron Microscopy Data Bank, codes  
205 EMD-3116, EMD-3117, EMD-3122 and EMD-3123.

206

## 207 **Results**

208

### 209 Architecture of *P. falciparum*-induced erythrocyte knobs

210 During blood stage development of the parasite, the most evident change to the erythrocyte  
211 cell surface is the appearance of the cytoadherent knobs<sup>10,12,13</sup>. In order to characterise knob  
212 structure, we processed synchronised late schizonts by high-pressure freezing and freeze  
213 substitution and examined sections of this material by electron microscopy. Knobs are visible  
214 as prominent protrusions on the surface of the erythrocyte membrane (Figure 1), as  
215 previously observed<sup>10,18,23,38–45</sup>. A layer of electron-dense material approximately 13 nm thick  
216 lies under the membrane in the knobs, about 10 nm below the membrane bilayer (Figure 1).  
217 It thus occupies a similar position to the erythrocyte cytoskeleton relative to the membrane<sup>46</sup>.  
218 The electron-dense material follows the shape of the knob in three dimensions (3D), forming  
219 cup-shaped structures ranging from 40-145 nm in diameter and averaging 50 nm in height  
220 (43 knobs examined).

221

### 222 A spiral structure underlies knobs

223 To obtain a more detailed view of the knob structure, we examined detergent-insoluble  
224 schizont skeletons by negative-stain electron microscopy. Knobs are visible as dark patches  
225 in the erythrocyte cytoskeleton, 70-100 nm in diameter (Figure 2). When this material is  
226 examined by electron tomography, structural components are resolved in 3D rather than  
227 being projected onto a single plane. In the resulting 3D reconstructions, knobs can clearly be  
228 seen to contain spirals made up of a stain-excluding filament 2-3 nm wide (Video S1). Figure 3  
229 A-C shows slices of these spirals at different depths through the knobs. Tracing these  
230 structures in 3D reveals that each knob contains a spiral filament that coils into a shallow

231 cone (Figure 3D,E, Video S1). Spirals turn anti-clockwise as viewed from the cytoplasmic  
232 (concave) side (Figure 3D,E, Figure S2). The spacing between turns of the filament varies from  
233 5-12 nm, and the gaps between turns contain a radiating structure with major radial features  
234 spaced approximately 4 nm apart (Figure 3A). A layer of more diffuse material, also having a  
235 radiating pattern, coats the upper surface of the conical frame formed by the spiral (viewed in  
236 different orientations in Figure 3C,F). When viewed from the side, this coating coincides with  
237 the cup-shaped structure seen as an electron-dense layer in resin-embedded sections  
238 (compare Figure 4A,B). This structure lies between the 2-3 nm spiral filament and the  
239 membrane, in cases where detergent extraction was incomplete (Figure 4B). The whole  
240 spiral-**plus-coat structure** (which we will refer to together as the knob skeleton) is 20-50 nm  
241 in height, similar to what was seen for resin-embedded material, suggesting that the negative  
242 stain procedure did not cause noticeable flattening. Knob density in the cytoskeleton was  
243  $11.8 \pm 5.1$  knobs/ $\mu\text{m}^2$ , which is similar to that reported for *P. falciparum* strains subjected to  
244 long-term *in vitro* culture as in this study <sup>47</sup>.

245

246 Knobs are embedded in the cytoskeleton and have a discontinuity at their apex

247 **To** examine the cytoskeleton in the hydrated state, we prepared frozen-hydrated schizont  
248 skeletons and imaged these by cryo-electron tomography (Figures 4C, 5; Video S3).  
249 Cytoskeleton and knobs can be seen clearly in the resulting cryo-tomograms (Figure 5A,C). It  
250 was possible to partially trace the path of the spirals, and to identify the coat on the outside of  
251 the spiral cone (Figure 5C). The **coat** coincides with the electron-dense layer in high-pressure  
252 frozen material and with the diffuse layer in negative stain (Figure 4). In cases where knobs  
253 present clear side views in the resulting cryo-tomograms, there is a discontinuity at the apex  
254 of the knob, with a break in the residual membrane in preparations where detergent  
255 extraction was incomplete (Figure 4C). This suggests a difference in membrane properties at  
256 this point, which could indicate the presence of specialised transmembrane components. In

257 Figure 5D, a model of the 3D structure traced from the 3D reconstruction (see Video S3) is  
258 superposed on a section of the density. Cytoskeletal filaments (blue) connect to the outside of  
259 the coat layer (magenta, Figure 5D). Points of contact between the cytoskeleton and coat layer  
260 (yellow spheres) are apparent over the whole surface of the coat layer, but most connections  
261 occur around the knob base (Figure 5E). No cytoskeletal material can be seen passing  
262 underneath the knobs (Video S3) in tomograms where the two apposed layers of the  
263 cytoskeleton, arising from the upper and lower cell surfaces, can be adequately distinguished.  
264 An anti-spectrin antibody labelled the erythrocyte skeleton of schizonts as expected, but  
265 labelling was almost completely excluded from regions within 50 nm of the centres of knobs  
266 (Figure S4). This suggests that spectrin, the major erythrocyte cytoskeletal building block, is  
267 excluded from the inside of the knobs, which were 70-100 nm in diameter. This supports the  
268 model described in Figure 5D,E, in which spectrin connects to the outer edges of knobs  
269 without passing underneath them. Importantly, outside of the knobs, there is no obvious  
270 qualitative difference in cytoskeleton structure between infected and uninfected erythrocyte  
271 skeletons (Figure 5A,B).

272

273 KAHRP is in the diffuse layer coating the spiral

274 Previous studies have demonstrated that the material underlying knobs contains KAHRP<sup>22,23</sup>.  
275 To locate KAHRP in the schizont skeletons, we used monoclonal antibodies (mAb) against  
276 KAHRP. Labelling was detected by negative-stain and cryo-electron tomography using a gold-  
277 conjugated secondary antibody (Figure 6). Skeletons labelled with anti-KAHRP antibody 18.2  
278 (Figure 6A,B) have gold beads clustered over the surface (Figure 6C,D), separated from the  
279 spiral by 10-60 nm (Figure 6E). Uninfected erythrocyte skeletons showed no labelling under  
280 identical conditions (Figure S5). A similar pattern of labelling was seen using anti-KAHRP  
281 antibody 89, which recognizes a different part of the KAHRP sequence (Figure S6). The  
282 epitope for mAb 18.2 is located in residues 282-362 of KAHRP, while that for mAb 89 lies

283 within residues 424-539 (Figure S6)<sup>48</sup>. These findings are in agreement with the earlier work  
284 and confirm that the knob skeletons contain KAHRP.

285

286 Membrane proteins are reorganised at knobs.

287 **T**o examine the distribution of proteins in the knob membrane, we used a custom-optimised  
288 system combining cryo-scanning electron microscopy (cryo-SEM) at ~2 nm resolution, with  
289 freeze-fracture. Freeze-fracture allows examination of the individual leaflets of the  
290 membrane bilayer, while this system facilitates visualisation over a fractured surface  
291 containing many thousands of schizonts at high magnification (Figure 7). Knobs appear as  
292 pits in the E-face (the inside of the outer membrane leaflet; Figure 7A) or protrusions in the P-  
293 face (the outside of the inner membrane leaflet; Figure 7B). Membrane proteins in the E-face  
294 are arranged in a mesh pattern that closely resembles the mesh of the cytoskeleton in  
295 dimensions and arrangement; knob protrusions show a circular clearing in this pattern with  
296 membrane proteins only remaining at the apex (Figure 7A). The dimensions of individual  
297 globular components in the pattern of membrane proteins range between 8-25 nm, including  
298 the 4 nm chromium coating. Membrane proteins in the P-face are smaller (approx. 5-10 nm)  
299 and appear less organised than in the E-face. However, a circular zone of clearing is also  
300 evident around the edges of the knob protrusions, similar to what was seen previously by low  
301 resolution freeze-fracture SEM of the P-face (Figure 7B)<sup>19,39</sup>. These findings demonstrate that  
302 the knob membrane has a distinct distribution of membrane proteins from the surrounding  
303 erythrocyte membrane, including a discrete structure at the apex.

304

305

## 306 **Discussion**

307

308 We have examined the cytoadherent knobs in *P. falciparum*-infected erythrocytes and have  
309 described a knob skeleton, containing a spiral structure, underlying the membrane  
310 protrusions (Figures 3,4). This structure is described schematically in Figure 7C. Armed with  
311 the present data, one can detect hints of the spiral structure in previously published images of  
312 purified knobs <sup>49</sup>. Our use of 3D imaging of schizont skeletons facilitated the interpretation of  
313 these structures as conical spirals.

314

315 The outer coat of the knob skeleton makes multiple connections to the surrounding  
316 erythrocyte cytoskeleton (Figure 5C-E; Video S3). These mechanical linkages suggest a means  
317 by which the shear forces involved in cytoadhesion by the knobs under flow conditions could  
318 be transmitted to the surrounding cytoskeleton (e.g., as discussed by <sup>18</sup>). A spiral support at  
319 the point of attachment might function in a spring-like fashion to absorb sudden changes in  
320 mechanical stress. Intrinsic flexibility in the structure that would support this idea is  
321 suggested by the variations observed in spacing between turns of the spiral.

322

323 Insertion of KAHRP-containing knobs into the cytoskeleton may also explain the rigidifying  
324 effect of KAHRP on the infected erythrocyte <sup>27</sup>. Knobs are present at high density on the  
325 surface of infected erythrocytes, and the numerous connections between the coat layer and  
326 the surrounding cytoskeleton are likely to have a significant impact on cytoskeletal  
327 mechanics. In clinical isolates, knob densities can reach up to four times what we observed in  
328 this laboratory strain <sup>47</sup>. These findings support the mechanism proposed in a recent  
329 modelling analysis for the rigidifying effect of the knobs on the erythrocyte cytoskeleton <sup>50</sup>.

330 Spectrin tetramers are capable of stretching to 194 nm in length <sup>51</sup>, which would allow for  
331 knob intercalation into the cytoskeleton mesh without further modification. It has been  
332 reported that the red cell cytoskeleton is gradually dismantled as the intracellular parasite  
333 develops <sup>42,52,53</sup>, and it is possible that some cytoskeletal connections are broken during knob

334 formation. However, in this study, which used highly synchronised, mature schizont  
335 preparations, no differences in cytoskeletal structure outside of the knobs were observed  
336 between uninfected erythrocyte skeletons and those from mature schizonts. These findings  
337 are not consistent with the notion of progressive degradation of the cytoskeleton.

338

339 Knobs are thought to comprise a complex of the cytoadherent ligand PfEMP1, KAHRP, other  
340 parasite-derived proteins and erythrocyte cytoskeleton components, such as spectrin, F-actin  
341 and ankyrin-R <sup>32,54–62</sup>. A central fragment of KAHRP containing lysine-rich repeat regions  
342 **forms** electron-dense patches under the membrane in resealed erythrocytes <sup>48</sup>, and full-length  
343 KAHRP expressed in *E. coli* forms clusters that associate with spectrin <sup>57</sup>. Our  
344 immunolabelling (Figure 6) strengthens earlier evidence localising KAHRP to the electron-  
345 dense layer underlying knobs <sup>22,23</sup>.

346

347 The distinctive spiral structure in the knobs (Figure 3) bears a striking resemblance to the  
348 structures formed by eukaryotic ESCRT-III proteins involved in ATP-driven intraluminal  
349 vesicle budding and membrane scission in mammalian and yeast cells <sup>63,64, 65–67</sup>. ESCRT-III  
350 proteins comprise alpha-helical bundles that assemble into a membrane-associated spiral <sup>63</sup>.  
351 While no homology could be detected between ESCRT-III proteins and any of the known  
352 components of knobs (Supporting Information S7), it is noteworthy that they both involve  
353 spiral structures of very similar appearance in membrane deformation. Only low levels of  
354 native ESCRT-III proteins have been detected in erythrocytes <sup>68</sup>. By comparison, knobs are  
355 present at high density in infected erythrocytes and also contain high concentrations of  
356 KAHRP <sup>12</sup>. The *P. falciparum* genome encodes five homologues of eukaryotic ESCRT-III  
357 proteins (PF08\_0064, PFI00300w, PFL2090c, PF14\_0397 and PF11\_0434; Supporting  
358 Information S7), all of which are expressed in the blood stages. However none of these is  
359 known or predicted to be exported to the erythrocyte cytoplasm (Supporting Information S7).

360 None of the knob-associated proteins is known to have ATPase activity, as might be expected  
361 for ESCRT-III complexes.

362

363 The erythrocyte membrane is modified considerably during *P. falciparum* infection by the  
364 insertion of parasite-derived proteins, including PfEMP1, as well as by changes in  
365 phosphorylation of cytoskeleton-associated proteins <sup>69–72</sup>. Phosphorylation of erythrocyte  
366 band 3 during infection has been shown to cause uncoupling of this cytoskeleton-organising  
367 transmembrane protein from the cytoskeleton <sup>73</sup>. We observed a rearrangement of  
368 transmembrane proteins at knobs by high-resolution, freeze-fracture cryo-SEM (Figure 7A,B).  
369 This is consistent with a role for knobs in organising and presenting transmembrane ligands  
370 on the erythrocyte surface <sup>18,19</sup>. In the E-face, knobs form prominent clearings in a network of  
371 membrane proteins, which are absent from all but the knob apex. A discontinuity was also  
372 observed at the apex of knobs in cryo-tomograms, consistent with a difference in the  
373 properties of the membrane at this point (Figure 4). Given that PfEMP1 has been clearly  
374 localised to the surface of knobs <sup>9,19</sup>, and that adhesion appears to occur at the apex of knobs  
375 in sections of infected cells adhering to the epithelial surface <sup>19</sup>, it seems likely that a PfEMP1-  
376 containing adhesive structure is located at the knob apex. Outside of the knobs, the network  
377 pattern of membrane proteins seen in the E-face by freeze-fracture SEM suggests that these  
378 may be cytoskeleton-associated, possibly band 3 or glycophorins (although there is some  
379 evidence that band 3 partitions preferentially with the P-face during fracture of uninfected  
380 erythrocytes <sup>74,75</sup>). Altered membrane protein distribution at knobs is less marked in the P-  
381 face, although there are clearings around knobs similar to those observed previously by SEM  
382 of freeze-fracture replicas <sup>19,39</sup>.

383

384 In conclusion, we have shown that erythrocyte knobs in *P. falciparum* infection contain a  
385 highly organised coated spiral structure underlying a specialised region of membrane (Figure



386 7C]. The application of electron tomography to schizont skeletons has revealed this  
387 previously undescribed knob skeletal framework. The observation of multiple connections  
388 between the knob skeleton and the erythrocyte cytoskeleton suggests a mechanical  
389 explanation for the cytoadherence-enhancing effects of knobs as well as for the reduction in  
390 cytoskeletal flexibility caused by knob components. The discovery of these structures  
391 suggests new avenues of research to elucidate the roles of individual components of the knob  
392 structure in antigen presentation and adherence.

393

## 394 **Acknowledgements**

395

396 We thank Kirsty MacLellan-Gibson for her assistance, and Andrew Osborne, Andrea Nans,  
397 Richard Hayward and Giulia Zanetti for helpful discussions. This work was supported by  
398 Medical Research Council Project Grant G1100013 (HRS, MJB, RAF), the EU FP7 NoE  
399 EviMalAR (MJB), the Wellcome Trust (088497/Z/09/Z (IV); PhD studentship (EEC);  
400 equipment grants 101488, 079605 and 086018 (HRS, MJB, RAF)) and the BBSRC (CASE PhD  
401 studentship BB/F016948/1 (VLH); equipment grant BB/L014211 (HRS)). We thank David  
402 Houldershaw and Richard Westlake for computing support, Peter Rosenthal for providing  
403 access to some facilities at the Francis Crick Mill Hill Laboratory, and Prof. Diane W. Taylor for  
404 her kind gift of anti-KAHRP mAb 89; mAb 18.2 was obtained from The European Malaria  
405 Reagent Repository (<http://www.malaria-research.eu>).

406

## 407 **Authorship contributions**

408 Contribution: J.M.W., I.V., R.A.F., M.J.B. and H.R.S. designed the research and wrote the  
409 manuscript; J.M.W, V.L.H, F.H, D.K.C and E.E.C. performed the research and collected data;  
410 J.M.W., V.L.H, I.V., R.A.F., M.J.B. and H.R.S. analysed and interpreted the data.

411

## 412 Disclosure of conflicts of interest

413 The PhD studentship of VLH was partly funded by Gatan, but the funders were not involved in  
414 planning the research. The authors declare that there were no other conflicts of interest.

415

416

417

## 418 References

- 419 1. World Health Organisation. World Malaria Report 2013. France: World Health  
420 Organisation; 2013.
- 421 2. Miller LH, Baruch DI, Marsh K, Doumbo OK. The pathogenic basis of malaria. *Nature*.  
422 2002;415(6872):673–9.
- 423 3. Chan J-A, Fowkes FJI, Beeson JG. Surface antigens of *Plasmodium falciparum*-infected  
424 erythrocytes as immune targets and malaria vaccine candidates. *Cell. Mol. Life Sci*.  
425 2014;71(19):3633–57.
- 426 4. Cooke B, Coppel R, Wahlgren M. Falciparum malaria: sticking up, standing out and out-  
427 standing. *Parasitol. Today*. 2000;16(10):416–20.
- 428 5. Ho M, White NJ. Molecular mechanisms of cytoadherence in malaria. *Am. J. Physiol*.  
429 1999;276(6 Pt 1):C1231–42.
- 430 6. Smith JD, Chitnis CE, Craig AG, et al. Switches in expression of *Plasmodium falciparum*  
431 var genes correlate with changes in antigenic and cytoadherent phenotypes of infected  
432 erythrocytes. *Cell*. 1995;82(1):101–110.
- 433 7. Flick K, Chen Q. var genes, PfEMP1 and the human host. *Mol. Biochem. Parasitol*.  
434 2004;134(1):3–9.
- 435 8. Hviid L. The role of *Plasmodium falciparum* variant surface antigens in protective  
436 immunity and vaccine development. *Hum. Vaccin*. 2010;6(1):84–9.
- 437 9. Baruch DI, Pasloske BL, Singh HB, et al. Cloning the *P. falciparum* gene encoding  
438 PfEMP1, a malarial variant antigen and adherence receptor on the surface of parasitized  
439 human erythrocytes. *Cell*. 1995;82(1):77–87.
- 440 10. Tilley L, Hanssen E. A 3D view of the host cell compartment in *P. falciparum*-infected  
441 erythrocytes. *Transfus. Clin. Biol*. 2008;15(1-2):72–81.

- 442 11. Nakamura K, Hasler T, Morehead K, Howard RJ, Aikawa M. *Plasmodium falciparum*-  
443 infected erythrocyte receptor(s) for CD36 and thrombospondin are restricted to knobs  
444 on the erythrocyte surface. *J. Histochem. Cytochem.* 1992;40(9):1419–22.
- 445 12. Kilejian A. Characterization of a protein correlated with the production of knob-like  
446 protrusions on membranes of erythrocytes infected with *Plasmodium falciparum*. *Proc.*  
447 *Natl. Acad. Sci. U. S. A.* 1979;76(9):4650–3.
- 448 13. Nagao E, Kaneko O, Dvorak JA. *Plasmodium falciparum*-infected erythrocytes:  
449 qualitative and quantitative analyses of parasite-induced knobs by atomic force  
450 microscopy. *J. Struct. Biol.* 2000;130(1):34–44.
- 451 14. Kriek N, Tilley L, Horrocks P, et al. Characterization of the pathway for transport of the  
452 cytoadherence-mediating protein, PfEMP1, to the host cell surface in malaria parasite-  
453 infected erythrocytes. *Mol. Microbiol.* 2003;50(4):1215–27.
- 454 15. Maier AG, Rug M, O'Neill MT, et al. Exported proteins required for virulence and rigidity  
455 of *Plasmodium falciparum*-infected human erythrocytes. *Cell.* 2008;134(1):48–61.
- 456 16. Waterkeyn JG, Wickham ME, Davern KM, et al. Targeted mutagenesis of *Plasmodium*  
457 *falciparum* erythrocyte membrane protein 3 (PfEMP3) disrupts cytoadherence of  
458 malaria-infected red blood cells. *EMBO J.* 2000;19(12):2813–23.
- 459 17. Langreth SG, Peterson E. Pathogenicity, stability, and immunogenicity of a knobless  
460 clone of *Plasmodium falciparum* in Colombian owl monkeys. *Infect. Immun.*  
461 1985;47(3):760–6.
- 462 18. Crabb BS, Cooke BM, Reeder JC, et al. Targeted gene disruption shows that knobs enable  
463 malaria-infected red cells to cytoadhere under physiological shear stress. *Cell.*  
464 1997;89(2):287–96.
- 465 19. Horrocks P, Pinches RA, Chakravorty SJ, et al. PfEMP1 expression is reduced on the  
466 surface of knobless *Plasmodium falciparum* infected erythrocytes. *J. Cell Sci.*  
467 2005;118(Pt 11):2507–18.
- 468 20. Cooke BM, Glenister FK, Mohandas N, Coppel RL. Assignment of functional roles to  
469 parasite proteins in malaria-infected red blood cells by competitive flow-based  
470 adhesion assay. *Br. J. Haematol.* 2002;117(1):203–11.
- 471 21. Ganguly AK, Ranjan P, Kumar A, Bhavesh NS. Dynamic association of PfEMP1 and  
472 KAHRP in knobs mediates cytoadherence during *Plasmodium* invasion. *Sci. Rep.*  
473 2015;5:8617.
- 474 22. Taylor DW, Parra M, Chapman GB, et al. Localization of *Plasmodium falciparum*  
475 histidine-rich protein 1 in the erythrocyte skeleton under knobs. *Mol. Biochem.*  
476 *Parasitol.* 1987;25(2):165–74.
- 477 23. Culvenor JG, Langford CJ, Crewther PE, et al. *Plasmodium falciparum*: identification and  
478 localization of a knob protein antigen expressed by a cDNA clone. *Exp. Parasitol.*  
479 1987;63(1):58–67.

- 480 24. Triglia T, Stahl HD, Crewther PE, et al. The complete sequence of the gene for the knob-  
481 associated histidine-rich protein from *Plasmodium falciparum*. *EMBO J*.  
482 1987;6(5):1413–9.
- 483 25. Hirawake H, Kita K, Sharma YD. Variations in the C-terminal repeats of the knob-  
484 associated histidine-rich protein of *Plasmodium falciparum*. *Biochim. Biophys. Acta*.  
485 1997;1360(2):105–8.
- 486 26. Marti M, Good RT, Rug M, Knuepfer E, Cowman AF. Targeting malaria virulence and  
487 remodeling proteins to the host erythrocyte. *Science*. 2004;306(5703):1930–3.
- 488 27. Glenister FK, Coppel RL, Cowman AF, Mohandas N, Cooke BM. Contribution of parasite  
489 proteins to altered mechanical properties of malaria-infected red blood cells. *Blood*.  
490 2002;99(3):1060–1063.
- 491 28. Acharya P, Chaubey S, Grover M, Tatu U. An exported heat shock protein 40 associates  
492 with pathogenesis-related knobs in *Plasmodium falciparum* infected erythrocytes. *PLoS*  
493 *One*. 2012;7(9):e44605.
- 494 29. Winter G, Kawai S, Haeggström M, et al. SURFIN is a polymorphic antigen expressed on  
495 *Plasmodium falciparum* merozoites and infected erythrocytes. *J. Exp. Med*.  
496 2005;201(11):1853–63.
- 497 30. Hinterberg K, Scherf A, Gysin J, et al. *Plasmodium falciparum*: the Pf332 antigen is  
498 secreted from the parasite by a brefeldin A-dependent pathway and is translocated to  
499 the erythrocyte membrane via the Maurer's clefts. *Exp. Parasitol*. 1994;79(3):279–91.
- 500 31. Proellocks NI, Herrmann S, Buckingham DW, et al. A lysine-rich membrane-associated  
501 PHISTb protein involved in alteration of the cytoadhesive properties of *Plasmodium*  
502 *falciparum*-infected red blood cells. *FASEB J*. 2014;28(7):3103–13.
- 503 32. Oberli A, Slater LM, Cutts E, et al. A *Plasmodium falciparum* PHIST protein binds the  
504 virulence factor PfEMP1 and comigrates to knobs on the host cell surface. *FASEB J*.  
505 2014;
- 506 33. Tarr SJ, Moon RW, Hardege I, Osborne AR. A conserved domain targets exported  
507 PHISTb family proteins to the periphery of *Plasmodium* infected erythrocytes. *Mol*.  
508 *Biochem. Parasitol*. 2014;196(1):29–40.
- 509 34. Yeoh S, O'Donnell RA, Koussis K, et al. Subcellular discharge of a serine protease  
510 mediates release of invasive malaria parasites from host erythrocytes. *Cell*.  
511 2007;131(6):1072–83.
- 512 35. Harris PK, Yeoh S, Dluzewski AR, et al. Molecular identification of a malaria merozoite  
513 surface sheddase. *PLoS Pathog*. 2005;1(3):241–51.
- 514 36. Mastronarde DN. Automated electron microscope tomography using robust prediction  
515 of specimen movements. *J. Struct. Biol*. 2005;152(1):36–51.
- 516 37. Mastronarde DN. Dual-axis tomography: an approach with alignment methods that  
517 preserve resolution. *J. Struct. Biol*. 1997;120(3):343–52.

- 518 38. Hanssen E, McMillan PJ, Tilley L. Cellular architecture of *Plasmodium falciparum*-  
519 infected erythrocytes. *Int. J. Parasitol.* 2010;40(10):1127–35.
- 520 39. Allred DR, Gruenberg JE, Sherman IW. Dynamic rearrangements of erythrocyte  
521 membrane internal architecture induced by infection with *Plasmodium falciparum*. *J.*  
522 *Cell Sci.* 1986;81:1–16.
- 523 40. Aikawa M. Morphological changes in erythrocytes induced by malarial parasites. *Biol.*  
524 *Cell.* 1988;64(2):173–81.
- 525 41. Sachanonta N, Chotivanich K, Chaisri U, et al. Ultrastructural and real-time microscopic  
526 changes in *P. falciparum*-infected red blood cells following treatment with antimalarial  
527 drugs. *Ultrastruct. Pathol.* 2011;35(5):214–25.
- 528 42. Cyrklaff M, Sanchez CPC, Kilian N, et al. Hemoglobins S and C interfere with actin  
529 remodeling in *Plasmodium falciparum*-infected erythrocytes. *Science.*  
530 2011;334(6060):1283–6.
- 531 43. Frankland S, Adisa A, Horrocks P, et al. Delivery of the malaria virulence protein  
532 PfEMP1 to the erythrocyte surface requires cholesterol-rich domains. *Eukaryot. Cell.*  
533 2006;5(5):849–60.
- 534 44. Bannister LH, Hopkins JM, Fowler RE, Krishna S, Mitchell GH. A brief illustrated guide to  
535 the ultrastructure of *Plasmodium falciparum* asexual blood stages. *Parasitol. Today.*  
536 2000;16(10):427–33.
- 537 45. Wickham ME, Rug M, Ralph SA, et al. Trafficking and assembly of the cytoadherence  
538 complex in *Plasmodium falciparum*-infected human erythrocytes. *EMBO J.*  
539 2001;20(20):5636–49.
- 540 46. Shahrokh Z, Verkman AS, Shohet SB. Distance between skeletal protein 4.1 and the  
541 erythrocyte membrane bilayer measured by resonance energy transfer. *J. Biol. Chem.*  
542 1991;266(18):12082–9.
- 543 47. Quadt KA, Barfod L, Andersen D, et al. The density of knobs on *Plasmodium falciparum*-  
544 infected erythrocytes depends on developmental age and varies among isolates. *PLoS*  
545 *One.* 2012;7(9):e45658.
- 546 48. Kilejian A, Rashid MA, Parra M, Yang YF. Sequence of the knob protein of *Plasmodium*  
547 *falciparum* recognized by a monoclonal antibody. *Mol. Biochem. Parasitol.*  
548 1991;48(2):231–3.
- 549 49. Chishti AH, Andrabi KI, Derick LH, Palek J, Liu S-CC. Isolation of skeleton-associated  
550 knobs from human red blood cells infected with malaria parasite *Plasmodium*  
551 *falciparum*. *Mol. Biochem. Parasitol.* 1992;52(2):283–287.
- 552 50. Zhang Y, Huang C, Kim S, et al. Multiple stiffening effects of nanoscale knobs on human  
553 red blood cells infected with *Plasmodium falciparum* malaria parasite. *Proc. Natl. Acad.*  
554 *Sci. U. S. A.* 2015;112(19):6068–6073.

- 555 51. Nans A, Mohandas N, Stokes DL. Native ultrastructure of the red cell cytoskeleton by  
556 cryo-electron tomography. *Biophys. J.* 2011;101(10):2341–50.
- 557 52. Millholland MG, Chandramohanadas R, Pizzarro A, et al. The malaria parasite  
558 progressively dismantles the host erythrocyte cytoskeleton for efficient egress. *Mol.*  
559 *Cell. Proteomics.* 2011;10(12):M111.010678.
- 560 53. Shi H, Liu Z, Li A, et al. Life cycle-dependent cytoskeletal modifications in *Plasmodium*  
561 *falciparum* infected erythrocytes. *PLoS One.* 2013;8(4):e61170.
- 562 54. Weng H, Guo X, Papoin J, et al. Interaction of *Plasmodium falciparum* knob-associated  
563 histidine-rich protein (KAHRP) with erythrocyte ankyrin R is required for its  
564 attachment to the erythrocyte membrane. *Biochim. Biophys. Acta.* 2014;1838(1):185–  
565 92.
- 566 55. Mayer C, Slater L, Erat MC, Konrat R, Vakonakis I. Structural analysis of the *Plasmodium*  
567 *falciparum* erythrocyte membrane protein 1 (PfEMP1) intracellular domain reveals a  
568 conserved interaction epitope. *J. Biol. Chem.* 2012;287(10):7182–9.
- 569 56. Voigt S, Hanspal M, LeRoy PJ, et al. The cytoadherence ligand *Plasmodium falciparum*  
570 erythrocyte membrane protein 1 (PfEMP1) binds to the *P. falciparum* knob-associated  
571 histidine-rich protein (KAHRP) by electrostatic interactions. *Mol. Biochem. Parasitol.*  
572 2000;110(2):423–8.
- 573 57. Oh SS, Voigt S, Fisher D, et al. *Plasmodium falciparum* erythrocyte membrane protein 1  
574 is anchored to the actin-spectrin junction and knob-associated histidine-rich protein in  
575 the erythrocyte skeleton. *Mol. Biochem. Parasitol.* 2000;108(2):237–247.
- 576 58. Waller KL, Nunomura W, Cooke BM, Mohandas N, Coppel RL. Mapping the domains of  
577 the cytoadherence ligand *Plasmodium falciparum* erythrocyte membrane protein 1  
578 (PfEMP1) that bind to the knob-associated histidine-rich protein (KAHRP). *Mol.*  
579 *Biochem. Parasitol.* 2002;119(1):125–9.
- 580 59. Cooke BM, Mohandas N, Coppel RL. Malaria and the red blood cell membrane. *Semin.*  
581 *Hematol.* 2004;41(2):173–188.
- 582 60. Kilejian A, Rashid MA, Aikawa M, Aji T, Yang YF. Selective association of a fragment of  
583 the knob protein with spectrin, actin and the red cell membrane. *Mol. Biochem.*  
584 *Parasitol.* 1991;44(2):175–81.
- 585 61. Pei X, An X, Guo X, et al. Structural and functional studies of interaction between  
586 *Plasmodium falciparum* knob-associated histidine-rich protein (KAHRP) and  
587 erythrocyte spectrin. *J. Biol. Chem.* 2005;280(35):31166–71.
- 588 62. Waller KL, Cooke BM, Nunomura W, Mohandas N, Coppel RL. Mapping the binding  
589 domains involved in the interaction between the *Plasmodium falciparum* knob-  
590 associated histidine-rich protein (KAHRP) and the cytoadherence ligand *P. falciparum*  
591 erythrocyte membrane protein 1 (PfEMP1). *J. Biol. Chem.* 1999;274(34):23808–23813.
- 592 63. Henne WM, Stenmark H, Emr SD. Molecular mechanisms of the membrane sculpting  
593 ESCRT pathway. *Cold Spring Harb. Perspect. Biol.* 2013;5(9):a016766.

64. Cashikar AG, Shim S, Roth R, et al. Structure of cellular ESCRT-III spirals and their relationship to HIV budding. *Elife*. 2014;e02184.
65. Bissig C, Gruenberg J. ALIX and the multivesicular endosome: ALIX in Wonderland. *Trends Cell Biol*. 2014;24(1):19–25.
66. Lata S, Schoehn G, Solomons J, et al. Structure and function of ESCRT-III. *Biochem. Soc. Trans*. 2009;37(Pt 1):156–60.
67. Solomons J, Sabin C, Poudevigne E, et al. Structural basis for ESCRT-III CHMP3 recruitment of AMSH. *Structure*. 2011;19(8):1149–59.
68. D'Alessandro A, Righetti PG, Zolla L. The red blood cell proteome and interactome: an update. *J. Proteome Res*. 2010;9(1):144–63.
69. Mbengue A, Yam XY, Braun-Breton C. Human erythrocyte remodelling during *Plasmodium falciparum* malaria parasite growth and egress. *Br. J. Haematol*. 2012;157(2):171–9.
70. Pantaleo A, Ferru E, Vono R, et al. New antimalarial indolone-N-oxides, generating radical species, destabilize the host cell membrane at early stages of *Plasmodium falciparum* growth: role of band 3 tyrosine phosphorylation. *Free Radic. Biol. Med*. 2012;52(2):527–36.
71. Pantaleo A, Ferru E, Carta F, et al. Analysis of changes in tyrosine and serine phosphorylation of red cell membrane proteins induced by *P. falciparum* growth. *Proteomics*. 2010;10(19):3469–79.
72. Roggwiler E, Bétoulle ME, Blisnick T, Braun-Breton C. A role for erythrocyte band 3 degradation by the parasite gp76 serine protease in the formation of the parasitophorous vacuole during invasion of erythrocytes by *Plasmodium falciparum*. *Mol. Biochem. Parasitol*. 1996;82(1):13–24.
73. Ferru E, Giger K, Pantaleo A, et al. Regulation of membrane-cytoskeletal interactions by tyrosine phosphorylation of erythrocyte band 3. *Blood*. 2011;117(22):5998–6006.
74. Fisher KA, Yanagimoto KC. Effect of membrane splitting on transmembrane polypeptides. *J. Cell Biol*. 1986;102(2):551–9.
75. Morrison M, Mueller TJ, Edwards HH. Protein architecture of the erythrocyte membrane. *Prog. Clin. Biol. Res*. 1981;51:17–34.

624

## 625 Figure legends

626 **Figure 1. Knobs in the membrane of a *P. falciparum*-infected erythrocyte have an**  
 627 **underlying electron-dense layer.** Average of 20 slices from a tomogram of a high-pressure

628 frozen, freeze-substituted schizont, showing knobs in the erythrocyte membrane and  
629 underlying electron-dense material. cyt, erythrocyte cytoplasm; mem, erythrocyte membrane;  
630 TVN/MC, tubulovesicular network/Maurer's cleft.

631

632 **Figure 2. Knobs are visible as dark patches in electron micrographs of detergent-**  
633 **extracted schizont skeletons.** Electron micrograph showing several knobs, indicated by  
634 arrowheads, in a negative-stained schizont skeleton, with surrounding cytoskeletal material.  
635 Inset: Two-fold enlarged view of the knob at top left.

636

637 **Figure 3. Knobs contain spiral structures seen in sections through three dimensional**  
638 **reconstructions.** A-C) Sections (averages of 3-4 slices) taken at different heights through  
639 knobs in a tomogram of a negative-stained schizont skeleton, showing a spiral structure.  
640 White arrows in A indicate some examples of radiating connections between turns; yellow  
641 arrows in C indicate diffuse coating material with a radiating pattern. D-E) Handedness and  
642 depth of knob spirals: models of two adjacent knobs from opposite sides of the skeleton,  
643 which have been collapsed onto one another during lysis and staining, viewed face-on (D) and  
644 from the side (E). F) Section through the tomogram tilted to cut through the coating layer of  
645 one side of a knob cone, showing coating material over at least five turns in curved layers  
646 (yellow arrows). Some stain-excluding membrane material (marked in F by a dashed line; see  
647 Fig. 4B) remains after detergent extraction.

648

649 **Figure 4. The electron-dense coating layer lies between the spiral and the membrane.**  
650 Comparison of side-view sections through knobs in tomograms of schizont material prepared



651 using different methods, showing layered arrangement of spiral, coat layer and membrane;  
652 averages of 10 tomographic slices through the knob apex. A) High pressure-frozen, freeze-  
653 substituted schizont showing membrane bilayer and underlying electron-dense material. B)  
654 Negative-stained detergent-insoluble schizont skeleton; contrast inverted to match A and C.  
655 The path of the spiral coil through the tomogram section is indicated by green circles. Some  
656 membrane remains after detergent extraction. View orthogonal to the plane of the tomogram.  
657 C) Schizont skeleton in vitreous ice, showing partially detergent-extracted membrane and  
658 underlying electron-dense material. A sharp discontinuity is present at the apex and in the  
659 coat layer.

660

661 **Figure 5. Knob skeletons make multiple connections to the erythrocyte cytoskeleton.**

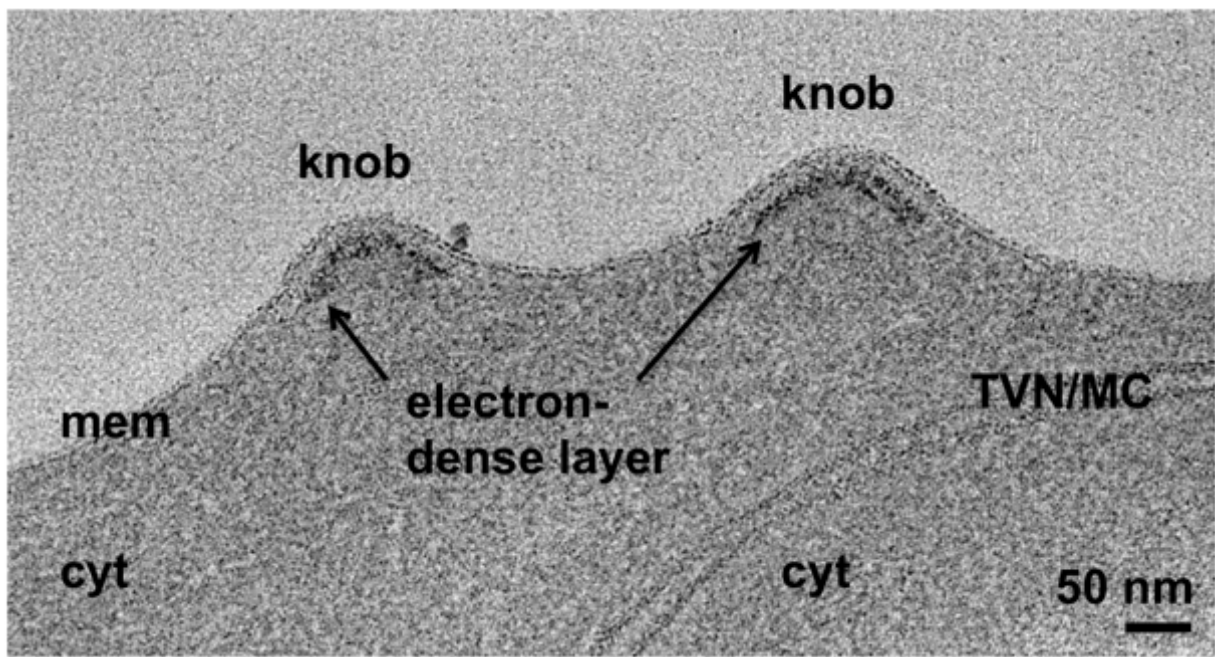
662 A) Schizont skeleton with knob skeletons in vitreous ice, average of 50 slices from an NAD-  
663 filtered cryo-tomogram. B) Uninfected erythrocyte skeleton, average of 30 slices. C) Enlarged  
664 view of boxed region in A, average of 30 slices, showing four knob skeletons and surrounding  
665 cytoskeleton. D) The same region shown in B, with superimposed model of knobs and  
666 associated material in 3D. Spiral strands are partially traced as green tubes and the coating  
667 layer of the knob skeletons is outlined by magenta contours. Points of connection with the  
668 surrounding cytoskeletal material (dark blue tubes) are marked by yellow spheres. E)  
669 Orthogonal views of a model of a typical knob skeleton (top right in C,D). In the side view  
670 (top), the estimated location of the cell membrane prior to detergent-extraction, based on  
671 Figure 4, is marked by a dashed line. The outer surface of the coat layer has been rendered as  
672 a mesh (magenta).

673

674 **Figure 6. Immuno-EM labelling of KAHRP in knob skeletons.** A). Thick section (average of  
675 50 slices) from a cryo-tomogram of schizont skeleton labelled with anti-KAHRP antibody 18.2  
676 and 10 nm gold-conjugated secondary antibody. B) The same field of view shown in A, with 70  
677 slices of a 3D model overlaid, describing knob spirals by the first and last turn (green  
678 contours), and gold beads as cyan spheres. C) Sections (30 slices each) through individual  
679 knobs in a cryo-tomogram of schizont skeleton labelled with mAb 18.2 and gold-conjugated  
680 secondary antibody, showing spiral structure with radiating pattern and gold labelling on the  
681 coat layer. Connected cytoskeleton is also visible. D) Model showing spirals as first and last  
682 turn (green contours) and gold label (cyan spheres) in a cryo-tomogram of schizont skeleton  
683 labelled with anti-KAHRP antibody 18.2. Dashed lines mark the boundaries in x of the volume  
684 shown in the side view. E) Chart showing the average density of gold beads at a given radial  
685 distance (in 3D) from knob spirals in four cryo-tomograms of schizont skeletons labelled with  
686 KAHRP antibody 18.2 and 10 nm gold-conjugated secondary antibody.

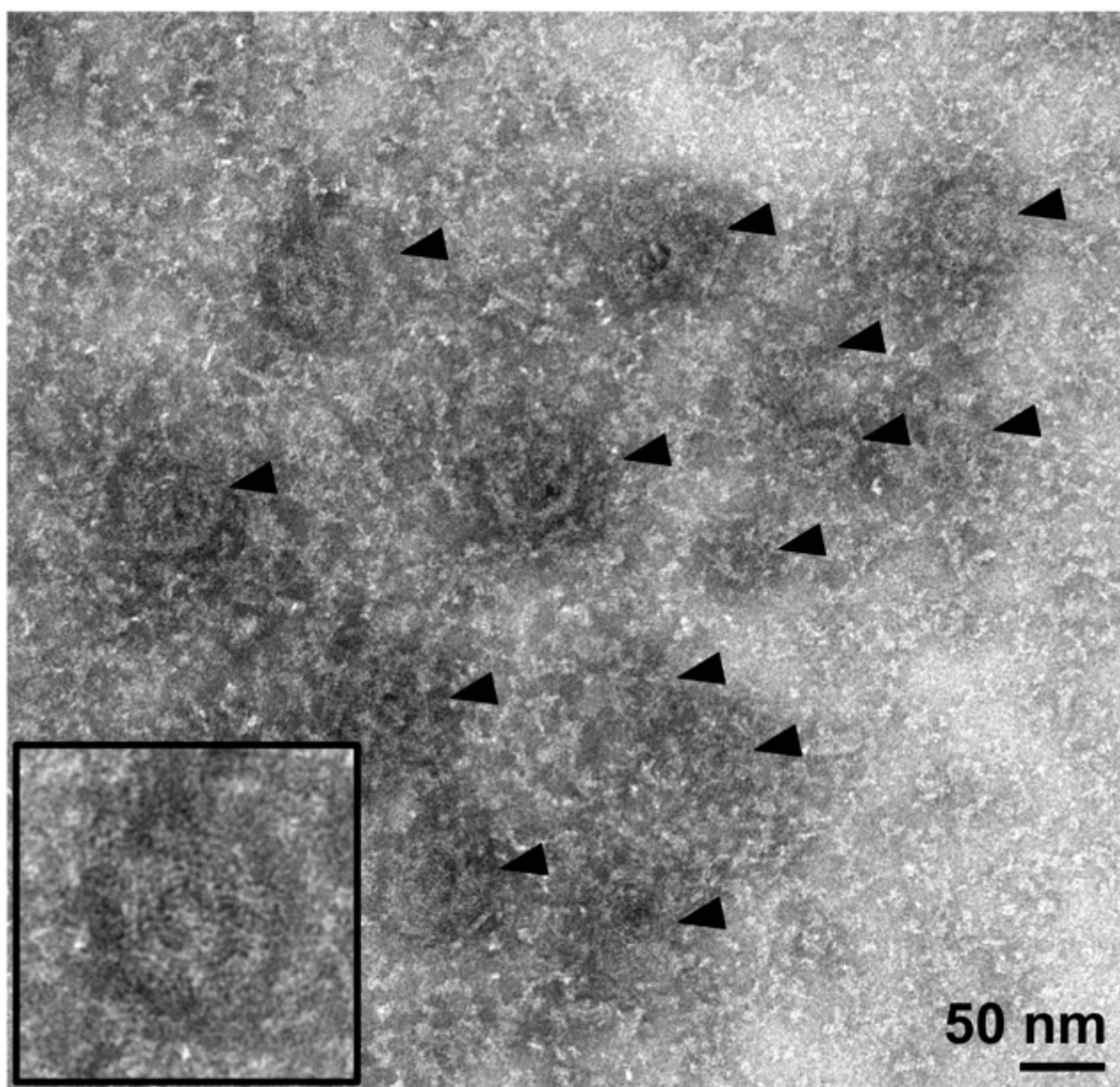
687  
688 **Figure 7. Knob membranes have a distinct distribution of membrane proteins.** Cryo-  
689 scanning electron microscopy images of freeze-fractured schizont coated with 4 nm  
690 chromium, showing erythrocyte membrane proteins. The knobs are clearly recognizable as  
691 indentations (A) or protrusions (B). Membrane proteins are visible as small lighter-shaded  
692 bumps forming various patterns on the surface. A) E-face (inside of the outer membrane  
693 leaflet). B) P-face (outside of inner membrane leaflet). Knobs are indicated by white  
694 arrowheads. C) Schematic of the knob structure, showing the spiral with coat layer underlying  
695 the erythrocyte membrane, and erythrocyte spectrin connecting to the outside of the coat  
696 layer. Membrane proteins are present at the knob apex and in the surrounding erythrocyte  
697 membrane, but are otherwise sparse in the knobs.

698  
699



700

701 **Figure 1.**



702

703 **Figure 2.**

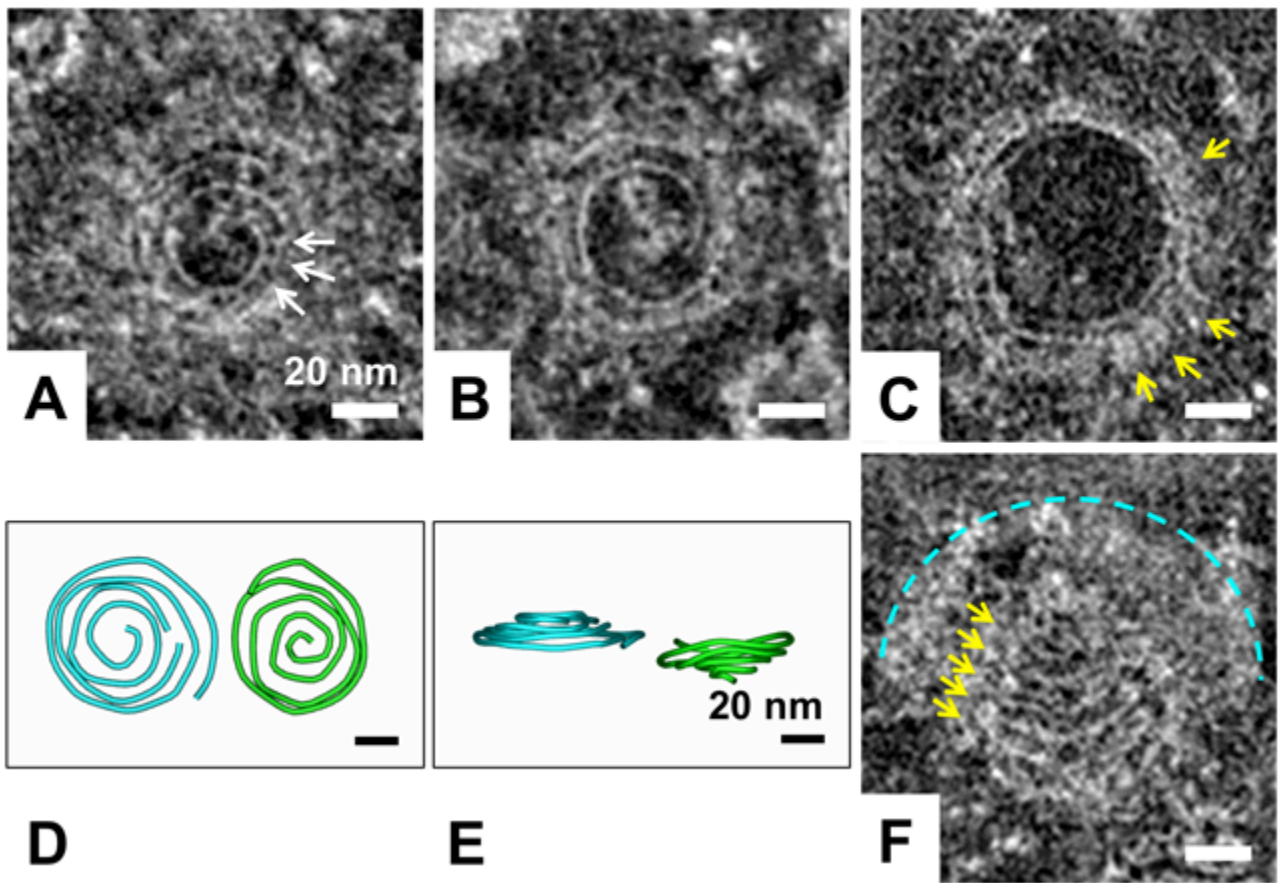
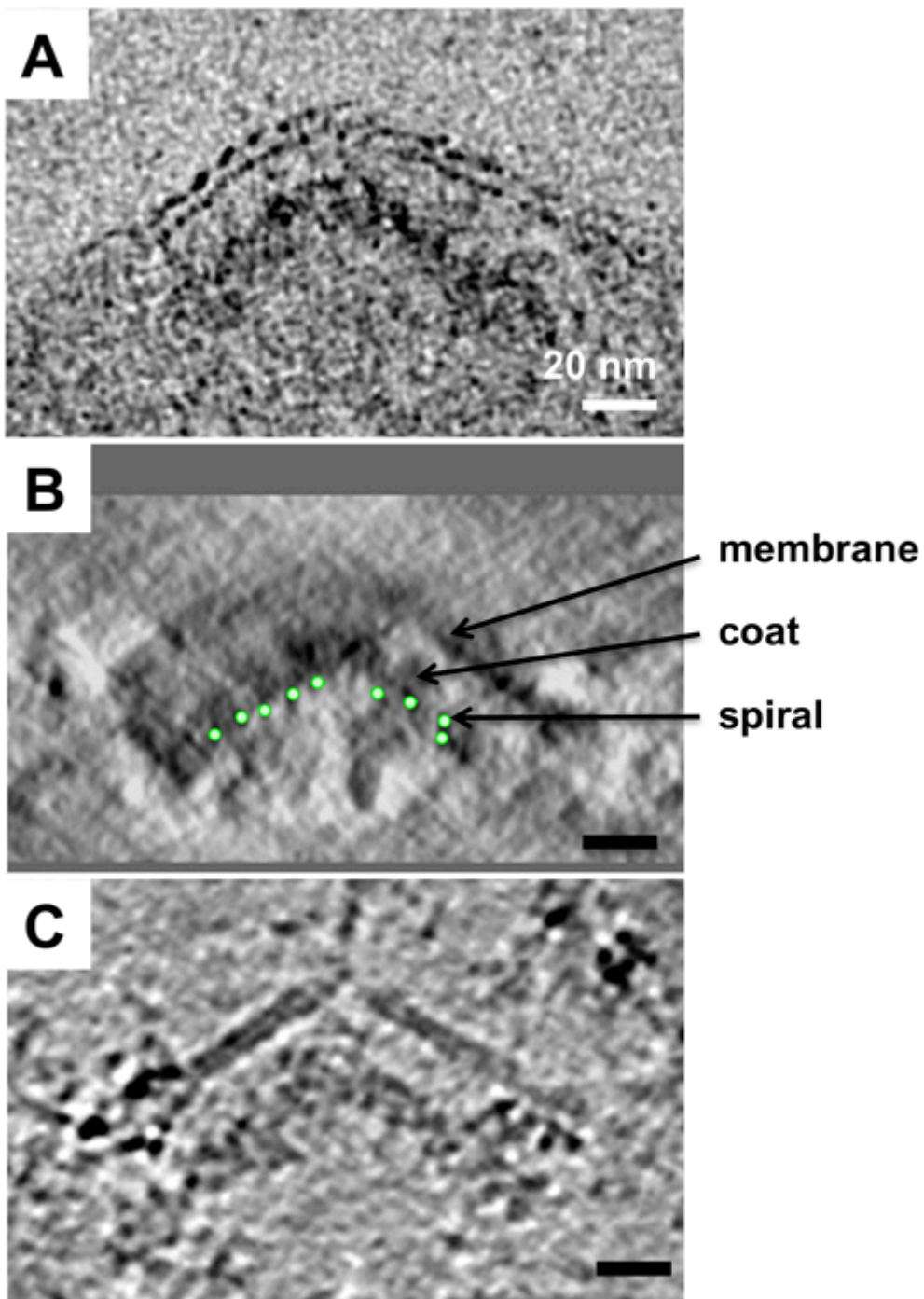
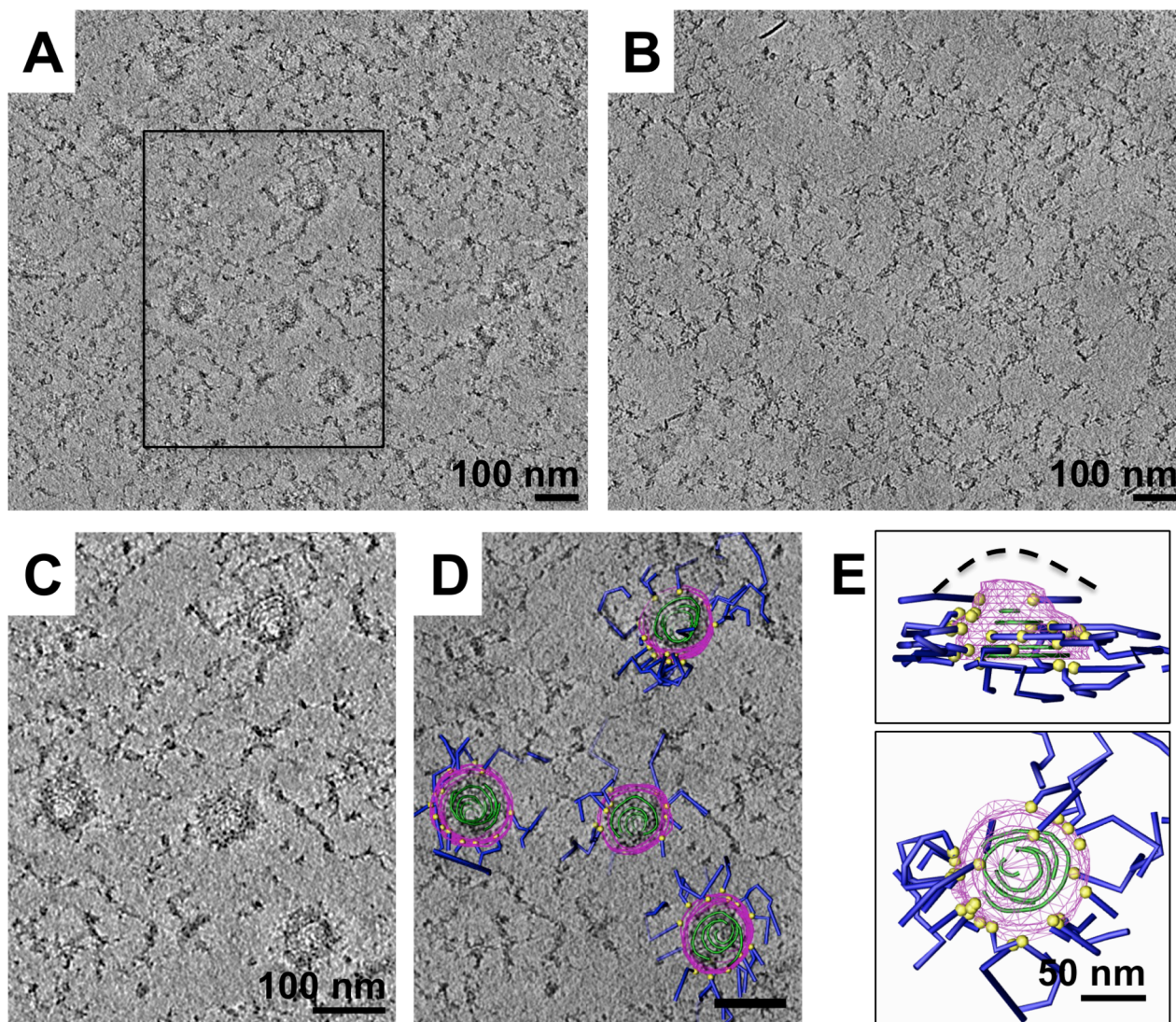


**Figure 3.**





706  
707 **Figure 4.**



708

709 **Figure 5.**



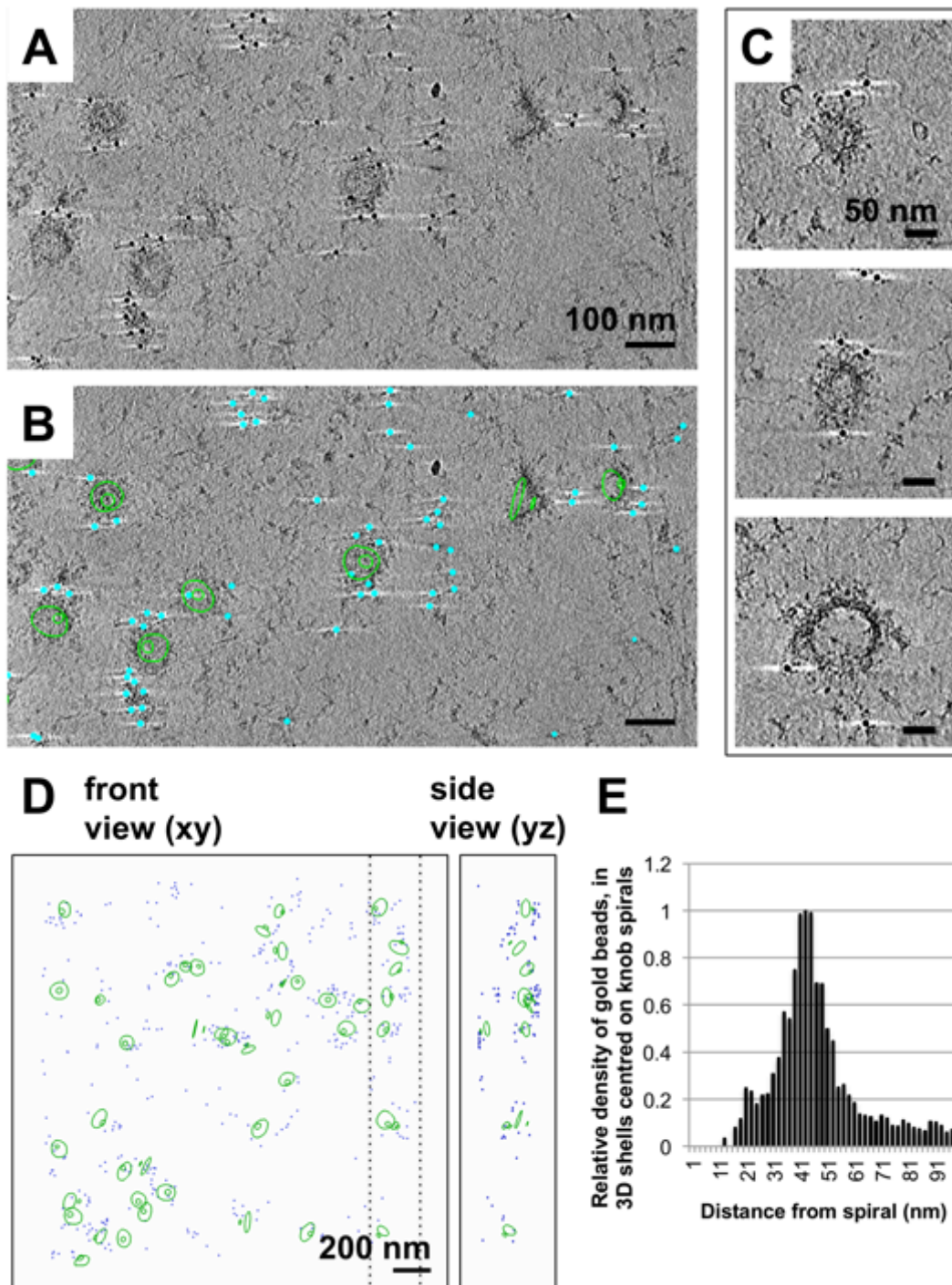
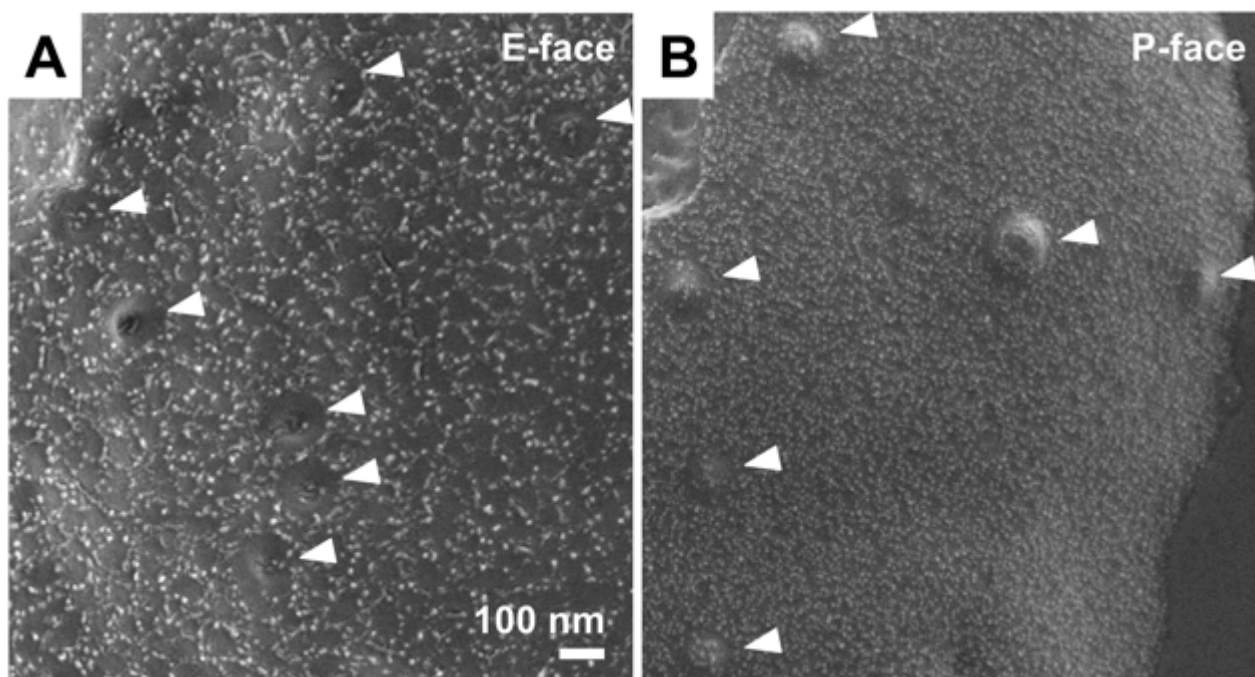


**Figure 6.**





**C**

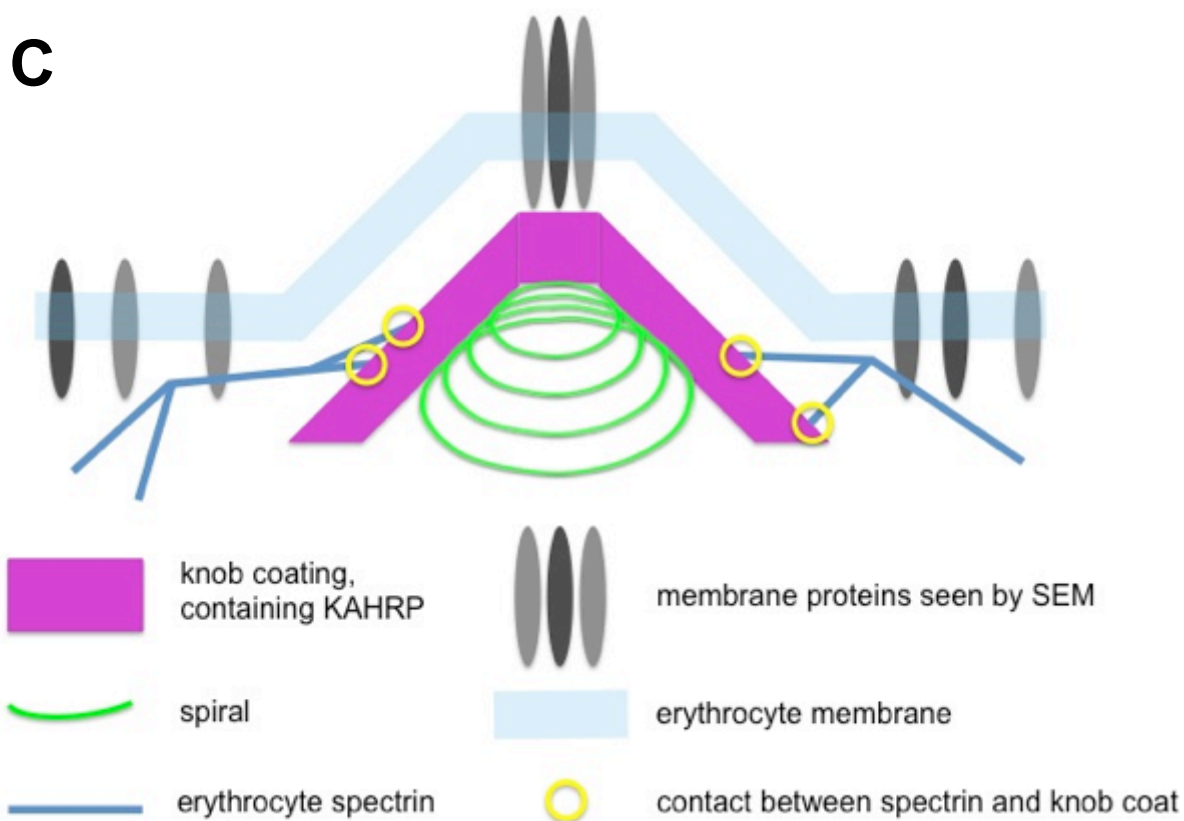


**Figure 7.**